Received August 2000
Revised February 2001
Accepted February 2001

Numerical natural convection in a sector-shaped enclosure

Joseph Sarr, Mactar Sall, Mamadou Mansour Kane
Centre d'Etudes et de Recherches sur les Energies Renouvelables, Université Cheikh Anta Diop de Dakar, Dakar, Sénégal
Bassirou Ba
Laboratoire des Semi-conducteurs et d'Energie Solaire, Faculté des Sciences et Techniques, Université Cheikh Anta Diop de Dakar, Dakar-Fann, Sénégal and
Michel Daguenet
Laboratoire de Thermodynamique et Energétique, Université de Perpignan, Perpignan, France

Keywords *Numerical methods, Enclosures, Natural convection, Flow*

Abstract *The purpose of this paper is to compare the numerical laminar two-dimensional unsteady natural convection in a partial sector-shaped enclosure submitted respectively to a constant heat flux density q1 and a uniform temperature T1 on the inner cylindrical wall. The numerical model performed in this paper is applied more particularly for high Grashof numbers, in order to point out the advent and the development of pre-turbulent flows. Results of numerical runs are presented. The mean Nusselt number on active walls is represented as a function of the Grashof number Gr and the aspect ratio F_r. The results may be correlated very well with an expression of the form $\overline{Nu} = k1\ Gr_1^{k2}$, for technical calculations.*

Nomenclature

Latin letters

a = parameter representing a length in the conformal transformation [m]
b = characteristic length of the problem [m]
F = symbolic function representing vorticity or temperature
F_r = aspect ratio of the studied enclosure Fr = Log(R_N/R_1) / ($\psi_M - \psi_1$)
g = gravitational acceleration [m s^{-2}]
G = symbolic parameter in the parabolic equation (6)
Gr = symbolic notation of the Grashof number (cases 1 and 2)
Gr_1 = modified Grashof number = g β b^4q1/($\nu^2\lambda$) (case 1)
Gr_2 = Grashof number = g β b^3(T1-T2)/ν^2 (case 2)
i = complex number such as $i^2 = -1$
kj = coefficients for equations (11) and (12)
M, N = grid points number in the angular and radial directions
Nu = Nusselt number
P = symbolic parameter in the parabolic equation (6)
Pr = Prandtl number = ν/α (= 0.72 in this paper)
q* = heat flux [W]
q1 = heat flux density imposed on inner cylindrical wall [W m^{-2}] (case 1)
R = radius of cylinder [m]
t = time [s]
T = temperature [K]
T0 = initial temperature [K]
T1 = temperature imposed on inner cylindrical wall [K] (case 2)
T2 = temperature imposed on outer cylindrical wall [K] (cases 1 and 2)

International Journal of Numerical Methods for Heat & Fluid Flow, Vol. 11 No. 4, 2001, pp. 342-357.

u, v = velocity components in the Cartesian system [m s^{-1}]
U,V = horizontal and vertical components of the velocity in the transformed field
x, y = coordinates in the Cartesian system [m]
z = complex variable

Greek letters
α = thermal diffusivity [m^2s^{-1}]
β = coefficient of thermal expansion [K^{-1}]
ΔGr = gradient of Grashof number
ΔNu = gradient of Nusselt number
Δt = time step
$\Delta\phi, \Delta\psi$ = grid spacings in ϕ and ψ directions respectively
λ = thermal conductivity [W $m^{-1}K^{-1}$]
ν = kinematic viscosity [m^2s^{-1}]
ρ = density [kg m^{-3}]
ψ = dimensionless angular coordinate in transformed field
ϕ = dimensionless radial coordinate in transformed field
Ω = Stream function, such that $u = \partial\Omega/\partial y$ and $v = -\partial\Omega/\partial x$ [m^2s^{-1}]
ω = vorticity = $\partial v/\partial x - \partial u/\partial y$ [s^{-1}]

Subscripts/superscripts
^{0} = value at initial time
^{1} = value on inner cylinder or on first adiabatic wall
$_{cond}$ = due to pure conduction
$_{dim}$ = dimension value
$_M$ = value on second adiabatic wall
$_{max}$ = maximum value
$_N$ = value on outer cylinder

Signs
$\overline{X}$ = average value
$\tilde{X}$ = dimensionless value

Introduction

Natural convection heat transfer within the annulus between two horizontal concentric cylinders has received wider attention because of its applications in energy conversion, storage and transmission.

There exists a number of studies concerning theoretical and experimental fluid flow and heat transfer in concentric cylindrical annuli. Vafai and Ettefagh (1991) studied numerically the buoyancy-driven flow and heat transfer in a horizontal annulus bounded by two impermeable boundaries in the axial direction. Castrejon and Spalding (1988) reported an experimental and numerical investigation of the transient free-convection flow in the annulus between horizontal concentric cylinders, the inner of which is being suddenly heated. A computational analysis of steady laminar natural convection of cold water within a horizontal annulus with constant heat flux on the inner wall and a fixed temperature on the outer surface was undertaken by Kumar (1988) in order to explore the occurrence of density inversion of water and its effects on the flow and temperature fields.

Only a few investigations in a partial sector shaped enclosure have been reported. In one such study, Al-Ani and Nansteel (1993) studied experimentally a fluid-filled sector where the radial surfaces were heated and cooled isothermally, while the remaining concentric walls were insulated. Sarr (1994) presented a numerical study of transient natural convection in an enclosure bounded by two horizontal concentric cylinders and two diametric planes. In this study, various boundary conditions were applied on solid walls. Sarr *et al.* (1995) reported investigations on an identical partial sector. In this work, a constant wall heat flux was applied on the inner cylinder, while the outer was maintained at a

uniform temperature, the other walls being adiabatic. Holographic interferometry was used to visualize the temperature field within the enclosure and to confirm the two-dimensional behavior of the convective flow.

In the present work a comparison is carried out about the laminar two-dimensional transient natural convection in a partial sector-shaped enclosure submitted respectively to a constant heat flux density q1 (case 1) and a uniform temperature T1 (case 2) on the inner cylindrical wall. In both these cases, the outer cylindrical wall is maintained at uniform temperature T2 and other walls are adiabatic (Figure 1).

The governing equations of motion and heat transfer are established within the Boussinesq approximation and the two-dimensional hypothesis and solved numerically through the vorticity-stream function approach. A conformal transformation (Lavrentiev and Chabat, 1972) is used to facilitate writing the expression for the boundary conditions. Relating to the numerical analysis, the discretization methods of various equations were already developed in a previous paper (Sarr *et al.,* 1995). Both the vorticity and energy were discretized by using the alternating direction implicit (ADI) method (Rao *et al.* (1985); Peaceman and Rachford (1955); Roache (1982); Carnahan *et al.* (1969)), while the stream function equation was solved by the successive over-relaxation (SOR) method (Bejan, 1984).

Problem formulation

To formulate the problem it is assumed that: the fluid is incompressible, viscosity is constant, density is considered as constant except in the equation of the motion. The fluid obeys the following Boussinesq approximation:

$$\rho = \rho_0[1 - \beta(\mathrm{T} - \mathrm{T0})] \tag{1}$$

In the energy equation, one neglects the pressure effect, the dissipation function and the radiation. The thermal conductivity is considered as constant. The problem is laminar two-dimensional and the study is realized in a normal plan to the axis of horizontal cylinders.

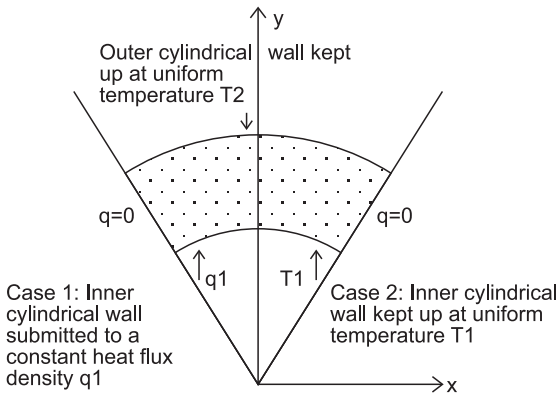

Figure 1.
Enclosure geometry in a Cartesian system

One can introduce the stream function $\Omega(x,y)$ and the vorticity $\vec{\omega}$ by the following relations:

$$u = \frac{\partial \Omega}{\partial y} \; ; \; v = -\frac{\partial \Omega}{\partial x} \; ; \; \vec{\omega} = \text{rot}\, \vec{V} = \omega \vec{k} = \left(\frac{\partial v}{\partial x} - \frac{\partial u}{\partial y}\right) \vec{k} \tag{2}$$

Conformal mapping

$$\begin{aligned} z &= a \exp(\phi + i\psi) = a \exp(\phi)(\cos \psi + i \sin \psi) \\ &= x + iy, \text{ with } i^2 = -1 \end{aligned} \tag{3}$$

Dimensionless quantities

$$\tilde{T} = \frac{g\beta b^3 Gr_1^{-3/4}}{\nu^2}(T - T2) \text{ and } Gr = Gr_1 = \frac{g\beta b^4 q1}{\nu^2 \lambda} \quad \text{(Case 1)}$$

$$\tilde{T} = \frac{g\beta b^3 Gr_2^{-3/4}}{\nu^2}(T - T0) \text{ and } Gr = Gr_2 = \frac{g\beta b^3 (T1 - T2)}{\nu^2} \quad \text{(Case 2)}$$

$$\tilde{\omega} = \frac{b^2 Gr^{-1/2}}{\nu}\omega \; ; \; \tilde{\Omega} = \frac{\Omega}{\nu} \; ; \; \tilde{t} = \frac{\nu Gr^{1/2}}{b^2} t$$

$$\tilde{U} = \frac{bGr^{-1/4}}{\nu} U \; ; \; \tilde{V} = \frac{bGr^{-1/4}}{\nu} V \; ; Pr = \frac{\nu}{\alpha} \; ; b = a\, Gr^{1/4} \tag{4}$$

The equations of mass, motion and energy become:

$$\tilde{\omega} = -\frac{1}{e^{2\phi}}\left(\frac{\partial^2 \tilde{\Omega}}{\partial \phi^2} + \frac{\partial^2 \tilde{\Omega}}{\partial \psi^2}\right) \tag{5}$$

$$\begin{aligned} &\frac{\partial F}{\partial \tilde{t}} + \frac{1}{e^{\phi}}\left(\tilde{U}\frac{\partial F}{\partial \phi} + \tilde{V}\frac{\partial F}{\partial \psi}\right) = \frac{G}{e_{\phi}}\left(\frac{\partial \tilde{T}}{\partial^{\phi}} \cos \psi - \frac{\partial \tilde{T}}{\partial \psi} \sin \psi\right) \\ &+ \frac{1}{\mathbf{P} \cdot \mathbf{e}^{2\phi}}\left(\frac{\partial^2 F}{\partial \phi^2} + \frac{\partial^2 F}{\partial \psi^2}\right) \end{aligned} \tag{6}$$

$$\text{with} : \tilde{U} = \frac{1}{e^{\phi}}\frac{\partial \tilde{\Omega}}{\partial \psi} \text{ and } \tilde{V} = -\frac{1}{e^{\phi}}\frac{\partial \tilde{\Omega}}{\partial \phi} \tag{7}$$

For motion equation : $F = \tilde{\omega}$; $G = 1$ and $P = 1$

For energy equation : F = $\tilde{T}$; G = 0 and P = Pr

Initial conditions
At $\tilde{t}$ = 0 the initial conditions are found to be:

$$\tilde{U} = \tilde{V} = 0, \tilde{\omega} = 0, \tilde{\Omega} = 0, \tilde{T} = \frac{g\beta b^3 Gr_1^{-3/4}}{\nu^2}(T0 - T2) \quad \text{(Case 1)} \tag{8}$$

$$\tilde{U} = \tilde{V} = 0, \tilde{\omega} = 0, \tilde{\Omega} = 0, \tilde{T}(\phi, \psi, 0) = 0 \quad \text{(Case 2)}$$

Boundary conditions

$$\tilde{U} = \tilde{V} = 0 \text{ on solid walls} \tag{9}$$

Flux and temperature conditions:

$$\frac{\partial \tilde{T}(\phi, \psi_1, \tilde{t})}{\partial \psi} = 0 \text{ and } \frac{\partial \tilde{T}(\phi, \psi_M, \tilde{t})}{\partial \psi} = 0 \tag{10}$$

$$\frac{\partial \tilde{T}(\phi_1, \psi, \tilde{t})}{\partial \phi} = -\exp(\phi_1) \text{ and } \tilde{T}(\phi_N, \psi, \tilde{t}) = \tilde{T}2 = 0 \text{ (Case 1)}$$

$$\begin{aligned} \tilde{T}(\phi_1, \psi, \tilde{t}) &= \frac{g\beta b^3 Gr_2^{-3/4}}{\nu^2}(T1 - T0)_{dim} \text{ and} \\ \tilde{T}(\phi_N, \psi, \tilde{t}) &= \frac{g\beta b^3 Gr_2^{-3/4}}{\nu^2}(T2 - T0)_{dim} \end{aligned} \quad \text{(Case 2)}$$

Nusselt numbers:

$$Nu(\phi_1, \psi) = \frac{\phi_N - \phi_1}{\tilde{\bar{T}}(\phi_N, \psi) - \tilde{T}(\phi_1, \psi)} \frac{\partial \tilde{T}(\phi_1, \psi)}{\partial \phi} \quad \text{(Case 1)}$$

$$\begin{aligned} Nu(\phi_1, \psi) &= \frac{\phi_N - \phi_1}{\tilde{T}2 - \tilde{T}1} \frac{\partial \tilde{T}(\phi_1, \psi)}{\partial \phi} \quad ; \\ Nu(\phi_N, \psi) &= \frac{\phi_N - \phi_1}{\tilde{T}2 - \tilde{T}1} \frac{\partial \tilde{T}(\phi_N, \psi)}{\partial \psi} \end{aligned} \quad \text{(Case 2)}$$

Numerical procedure

The various equations of the phenomenon are solved by considering a rectangular network of N nodes along the ϕ axis and M nodes along the ψ axis.

$\Delta\phi$ and $\Delta\psi$ are chosen as grid spacings respectively in the two preceding directions.

The stream function equation is solved by using the SOR method (successive over-relaxation) that allows a very quick convergence of calculations after 15 to 25 iterations.

The motion and energy equations are discretized in two half-times according to the alternating direction implicit method (ADI). Already used by Peaceman and Rachford in 1955, this method consists of discretizing over two consecutive time half-steps, two implicit difference equations alternately versus ϕ and ψ directions. The obtained equations afford, as a result, when they are applied to each node, two tridiagonal equations systems that can be solved by the elimination method of Thomas (Gourdin and Boumahrat, 1983).

Results and discussions

Accuracy of calculations

The convergence of the steady-state solution was verified by checking the balance between the mean Nusselt number variation at the inner and outer cylindrical walls within 1 per cent. Various grids from 21 (radial) $\times$ 21 (angular), 31 $\times$ 21 to 31 $\times$ 81 in the ϕ-direction and from 21 $\times$ 21, 21 $\times$ 51 to 81 $\times$ 51 in the ψ-direction were considered for the grid size study. The results reported in the paper were mainly obtained with the grids ranging from 21 $\times$ 21 to 31 $\times$ 51, depending on the aspect ratio and the Grashof number, which were considered to represent a reasonable compromise between accuracy and computing cost. For instance, as shown in Figure 2, respectively for $F_r = 1/2$ and $Gr_1 = 10^6$ (case 1) and for $F_r = 1/2$ and $Gr_2 = 10^4$ (case 2), the difference in the mean Nusselt number is less than 0.3 per cent between using the 31 $\times$ 51 and 31 $\times$ 81 grids and less than 0.6 per cent between using the 31 $\times$ 51 and 81 $\times$ 51 grids. The numerical computations have been carried out on a Pentium Compaq. The CPU time required generally depends on the problem. For example, for a Grashof number of 10^6 and $F_r = 1/2$, 1 hour 35 minutes of CPU time was required to reach convergent and steady-state solution, with the basic grid of 31 $\times$ 51.

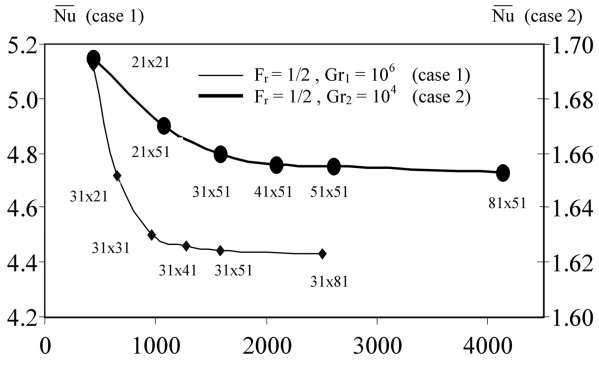

Figure 2.
Variations of mean Nusselt number vs. grid system: N (radial) $\times$ M (angular)

The time and the storage required were respectively about 1.2 s per time step and 3,132 Ko.

Field investigated

To illustrate this study, we executed the calculation program for various aspect ratios and Grashof numbers, marked hereafter :

- Case 1: $F_r = 1/1, F_r = 1/2, F_r = 1/3, F_r = 1/5$ and $100 \leq Gr_1 \leq 10^8$
- Case 2: $F_r = 1/2, F_r = 1/3, F_r = 1/5$ and $100 \leq Gr_2 \leq 10^7$, $F_r = 1/1$ and $100 \leq Gr_2 \leq 10^6$.

As the Grashof number increases, the flow becomes stronger. The resulting flow, which is complex, exhibits a steady-oscillatory behavior rather than a fully time-invariant one. The average Nusselt number fluctuates on both cylindrical surfaces, with a bigger amplitude for case 2. Thus, in this case, for $F_r = 1/1$ and for $Gr_2 > 10^6$, the calculation model becomes inconvenient.

Study of case 1

Figures 3 and 4 show the temperature and the stream function distribution respectively in terms of isotherms and streamlines in the cavity studied, for very high Grashof numbers, with respect to the time evolution. The streamlines and the isotherms shown in each frame of preceding figures are selected in order to best visualize the flow field and do not correspond necessarily to equally-spaced values. In each of the cross-sectional representations, the streamlines are plotted in the left half and the isotherms in the right half. These curves are symmetrical about the vertical radius of the cavity. The heat transfer for each wall can be evaluated from temperature distributions.

At the beginning (Figures 3a, 4a), only a thin fluid layer is heated in the vicinity of the inner cylindrical wall, when this wall is suddenly heated; a boundary layer is forming, inside which the temperature gradients are localized. The isotherms are then parallel to the heated wall. This is because the flow velocity is too small to affect the temperature distribution and consequently the heat transfer mechanism is mainly by conduction. For all configurations investigated, the flow is two-cellular at very early times.

With time increasing, when convective motions are present (Figures 3b-f and 4b-d), the heat flux is carried by conduction and by convection which produce a distortion of the isothermal lines. The streamlines always form at the outer corners of the inner cylindrical wall. They expand with time and move towards the midst of the fluid before becoming round in shape. Later, these curves flatten themselves against the walls and the symmetrical axis, and generate consequently a thermal boundary layer near the region of high heat transfer.

For $F_r = 1/2, 1/3, 1/5$, the flow remains always two-cellular. The motion is induced by fluid particles heated by the inner cylinder. These particles become lighter and go up to the isothermal wall along the symmetrical axis. They are cooled on this wall and go down hugging the walls. Two eddies rotating in opposite directions are thus obtained. One should note the outbreak and the

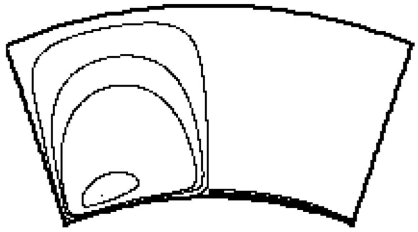

(a) $\tilde{t} = 10$

$\tilde{\Omega}$: 9.56, 7.50, 1.50, 0.75, 0.15

$\tilde{T}$ bottom-->top : 4.2, 4.0, 3.0, 2.0, 1.0

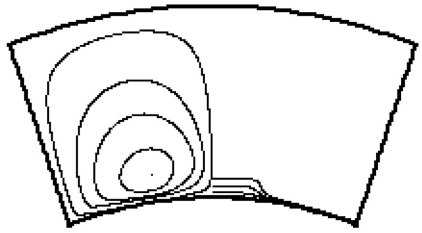

(b) $\tilde{t} = 20$

$\tilde{\Omega}$: 43.47, 30.00, 15.00, 7.50, 1.50

$\tilde{T}$ bottom-->top : 6.5, 5.0, 3.0, 2.0, 1.0

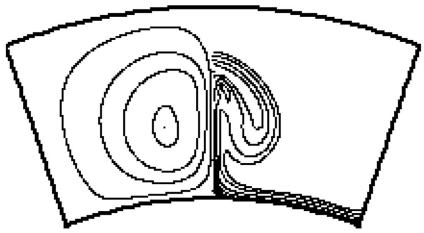

(c) $\tilde{t} = 30$

$\tilde{\Omega}$: 149.28, 135.0, 75.0, 45.0, 15.0

$\tilde{T}$ bottom-->top : 7.0, 6.0, 5.0, 4.0, 3.0, 2.0, 1.0, 0.5

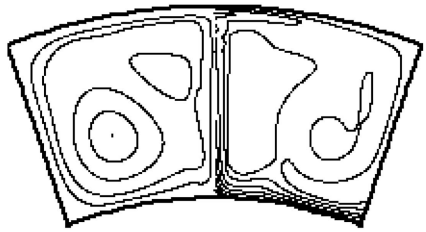

(d) $\tilde{t} = 70$

$\tilde{\Omega}$: 134.4, 112.5, 75.0, 37.5, 15.0

$\tilde{\Omega}$ upper cell : 37.5

$\tilde{T}$ bottom-->top : 8.0, 6.0, 5.0, 4.0, 3.0, 2.0, 1.0, 0.5 / $\tilde{T}$ cells (left-->right) : 0.5, 1.0

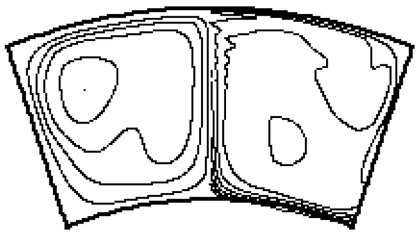

(e) $\tilde{t} = 90$

$\tilde{\Omega}$: 152.55, 120.0, 75.0, 45.0, 15.0

$\tilde{T}$ bottom-->top : 8.0, 6.0, 5.0, 4.0, 3.0, 2.0, 1.0, 0.5 / $\tilde{T}$ cell : 0.5

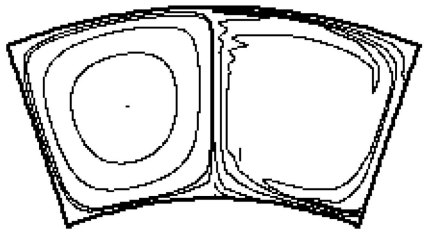

(f) $\tilde{t} = 1200$

$\tilde{\Omega}$: 213.45, 150.0, 75.0, 15.0, 7.5

$\tilde{T}$ bottom-->top : 9.0, 7.0, 5.0, 3.0, 2.2, 2.0, 1.7, 1.0

Figure 3.
Variation of streamlines and isotherms versus dimensionless time for $F_r = 1/2$ and for $Gr_1 = 10^8$ (case 1)

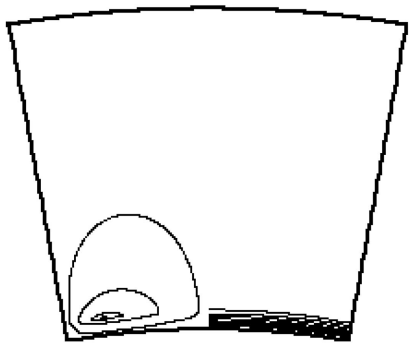

(a) $\tilde{t} = 0.01$

$\tilde{\Omega}$: 1.30, 1.20, 0.75, 0.15

$\tilde{T}$ bottom-->top : 2.0, 1.8, 1.6, 1.4, 1.2, 1.0, 0.8, 0.6, 0.4, 0.2

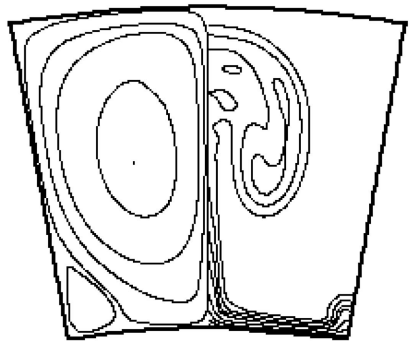

(b) $\tilde{t} = 40$

$\tilde{\Omega}$ (upper cells) : 159.75, 112.5, 37.5, 15, 1.5

$\tilde{\Omega}$ (lower cell) : -1.5

$\tilde{T}$ bottom-->top : 6.0, 5.0, 4.0, 3.0, 2.0, 1.5, 1.0, 0.5

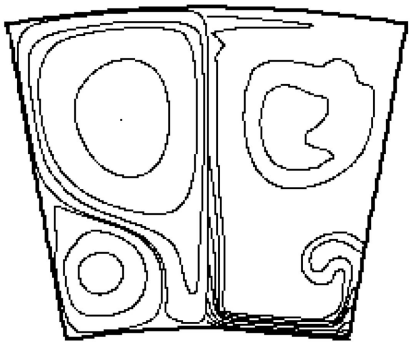

(c) $\tilde{t} = 50$

$\tilde{\Omega}$ (upper cells) : 166.95, 112.5, 37.5, 15, 1.5

$\tilde{\Omega}$ (lower cells) -37.5, -15.0, -1.5

$\tilde{T}$ bottom-->top : 6.0, 5.0, 4.0, 3.0, 2.0, 1.5, 1.0, 0.5; $\tilde{T}$ cells (inner-->outer) : 1.0, 0.5

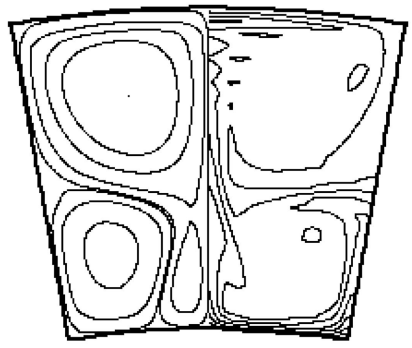

(d) $\tilde{t} = 150$

$\tilde{\Omega}$ (upper cells) : 122.4, 75.0, 45.0, 15.0, 1.5

$\tilde{\Omega}$ (lower cells, left) : -45.0, -15.0, -1.5

$\tilde{\Omega}$ (lower cells, right) : 15.0, 1.5

$\tilde{T}$ bottom-->top : 6.0, 5.0, 4.0, 3.0, 2.0, 1.5, 1.0, 0.5

Figure 4.
Variation of streamlines and isotherms versus dimensionless time for $F_r = 1/1$ and for $Gr_1 = 10^8$ (case 1)

disappearance of secondary eddies with low intensity located in the main cells. These secondary eddies turn in the same direction as principal ones. This development is illustrated in Figure 3d for $F_r = 1/2$ and $Gr_1 = 10^8$. The appearance of unstable secondary cells points to the setting-up of a pre-turbulent flow which disappears at the approach of the steady state. The development of the pre-turbulent state described above is also shown by the presence of closed lines as isotherms wholly located within the fluid.

For $F_r = 1/1$, when the flow is four-cellular (steady state streamlines and isotherms pattern not shown in this paper), there are initially two eddies rotating in contact with the inner cylinder and, as time increases, two additional eddies, turning in the opposite direction to the neighboring cells, establish themselves at the lower corners of the enclosure (Sarr, 1994). A similar behavior was reported by Rao *et al.* (1985) for annuli. For $F_r = 1/1$ and for higher Grashof numbers, the streamlines split up later into several adjoining eddies turning in the opposite direction, on both sides of the symmetrical plane of the cavity, as time increases. This result is illustrated in Figure 4, where the appearance of two and later three eddies is pointed out, corresponding respectively to a four- and a six-cellular flow pattern. This is due to the setting-up of an oscillatory transient phenomenon, which is a transition towards a mainly turbulent flow (Fukuda *et al.*, 1990). For high Grashof numbers, oscillatory flow appears. The observation of isotherms and streamlines on Figure 4-d shows that the heat transfers are more intense in the areas in which the particles in movement come into contact with the active walls. These transfers are also important inside the enclosure, in the areas where the fluid particles of lower and upper cells conjoin. For $F_r = 1/1$, one can consider that the appearance of additional cells, when the Grashof number is raised, creates inside the fluid an area of thermal transfer between the upper cells and the lower cells.

The oscillatory phenomenon previously brought to the fore is better pointed out by plotting the maximum value of the stream function $\tilde{\Omega}_{max}$ and the mean Nusselt number vs. time in Figure 5, for $F_r = 1/1$ and $Gr_1 = 10^8$. With time increasing, these functions are oscillating about mean values (for $\tilde{t} \geq 220$, $\overline{Nu} = 14.4 \pm 1.8$). As the Grashof number is increased further, the oscillatory flow gradually loses its periodicity and exhibits a turbulent behavior. For $F_r = 1/2$ and $Gr_1 = 10^8$, the oscillatory flow is followed by a steady state regime (Figure 6).

Figure 7 describes the average variations of the mean Nusselt number on the active walls vs. Gr_1 and F_r respectively, at the steady state. For configurations studied, this Figure shows clearly that, for small modified Grashof numbers, the heat flux is only due to the conduction ($\overline{Nu} = 1$). If the variations of the mean Nusselt number vs. modified Grashof number are represented in a log-log scale (Figure 8), one observes that the curves remain practically horizontal up to a Grashof number equal to 1,000, corresponding approximately to the superior limit of the conduction dominating regime. For $Gr_1 \geq 1{,}000$, when the motion is present, the fluid velocity entails a supplementary heat flux due to the convection, and the total heat flux is higher than only for the conduction regime

($\overline{Nu} > 1$). The effect of the flow rate change, which corresponds to the change from the two-cellular to the four-cellular flow and now to the six-cellular flow, appears clearly in this Figure. Indeed, when the curves are always made up of two branches for the aspect ratios 1/2, 1/3 and 1/5, the curve representing the aspect ratio $F_r = 1/1$ presents a third branch (for $10^5 \leq Gr_1 < 7 \times 10^5$) and then a fourth branch (for $Gr_1 \geq 7 \times 10^5$), with increasing Gr_1.

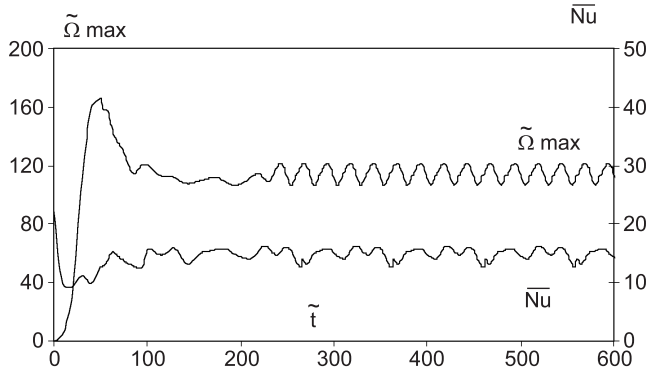

Figure 5.
Variation of maximum stream function and mean Nusselt number versus dimensionless time for $F_r = 1/1$ and $Gr_1 = 10^8$ (case 1)

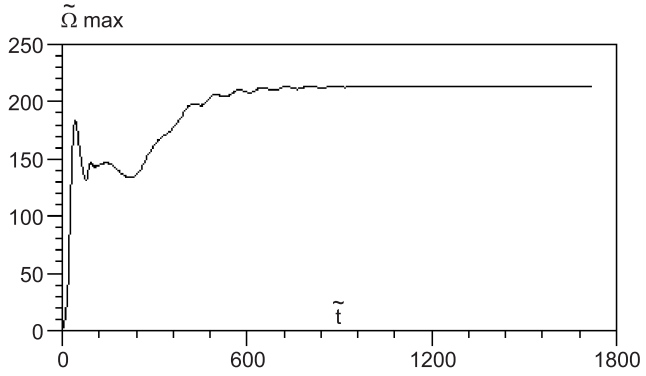

Figure 6.
Variation of maximum stream function versus dimensionless time for $F_r = 1/2$ and $Gr_1 = 10^8$ (case 1)

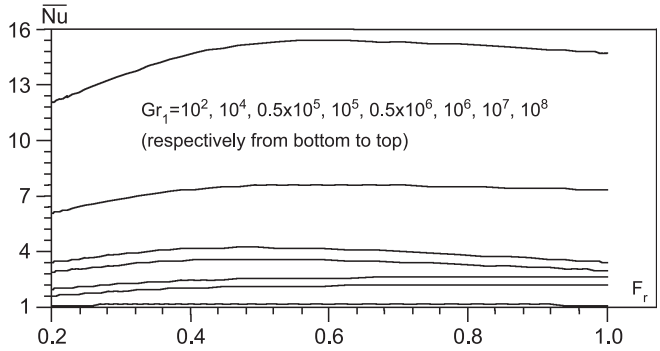

Figure 7.
Variations of mean Nusselt number on cylindrical walls versus aspect ratios for different modified Grashof numbers (case 1)

These observations confirm therefore the appearance and the development of one or several localized disturbances on the inner cylindrical wall, for $F_r = 1/1$ (Sarr, 1995). These disturbances, that correspond to a change of the flow rate, show themselves by the variation of the heat transfer gradient on the active walls of the enclosure, according to the two-, four- or six-cellular character of the convective flow. The presence of positive counter-clockwise cells on the left part of the inner cylinder is conducive to the increase of the average Nusselt change with respect to the Grashof number $\Delta\overline{Nu}/\Delta Gr_1$, contrary to the negative clockwise cells.

One can deduct from these results that, for Grashof numbers greater than 1,000, thermal-convective exchanges are better when the aspect ratio is increased from 1/5 to 1/2. For $F_r = 1/1$, one can consider that the appearance of the four additional cells, when the Grashof number is raised, creates inside the fluid a thermal transfer area between the upper cells and the lower cells. A thermal exchange is, moreover, developed between the lower left cells and the right ones.

To allow the integration of these results in thermal calculations, the mean Nusselt number is represented by an expression of the following form:

$$\overline{Nu} = k1\ Gr_1^{k2} \tag{11}$$

The values of the coefficients k1 and k2 corresponding to the investigated aspect ratios and the validity domains of the preceding formula are presented in Table I.

Study of case 2

The summary of principal numerical runs is presented in Table II.

The analysis of obtained results allows us to assert that the nature of the flow is qualitatively the same as the one in case 1. For $F_r = 1/2$, 1/3 and 1/5, the flow remains two-cellular. For $F_r = 1/1$ and for $Gr_2 < 6 \times 10^4$, the flow is also two-cellular. For $F_r = 1/1$ and for $Gr_2 \geq 6 \times 10^4$, additional eddies turning in the opposite direction to the neighboring cells establish themselves at the lower corners of the enclosure with time increasing.

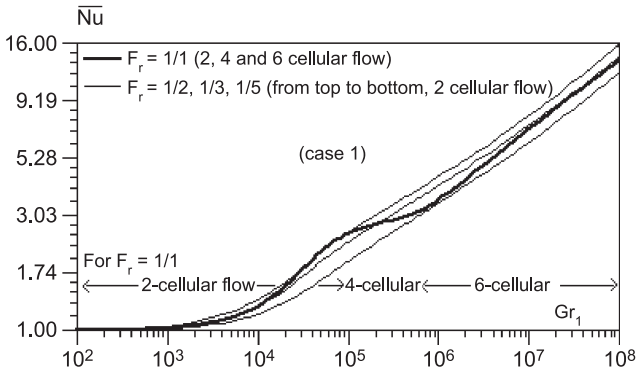

Figure 8.
Variations of mean Nusselt number on isothermal walls versus modified Grashof numbers for different aspect ratios

The unsteady flow patterns for $F_r = 1/1$ and $Gr_2 = 10^6$ are presented in Figure 9, in which the six-cellular feature of the flow is shown at $\tilde{t} = 150$ (Figure 9d). This trend corresponds to the oscillatory flow which could be better indicated by plotting the maximum value of the stream function $\tilde{\Omega}_{max}$ vs. time (Figure 10).

In Figure 11 representing the variations of the mean Nusselt number on the isothermal walls vs. Gr_2, one observes the same behavior as for case 1. The curve representing $F_r = 1/1$ presents a third branch from $Gr_2 = 6 \times 10^4$ and a fourth branch for $Gr_2 \geq 5 \times 10^5$. The presence of these third and fourth curve branches is naturally the consequence of a change in the nature of the flow and corresponds to the development of the four-cellular and the six-cellular flow respectively inside the fluid.

It is possible, as for the case 1 study, to represent the mean Nusselt number by an expression of the form:

$$\overline{Nu} = k3\ Gr_2^{k4} \tag{12}$$

F_r	1/1	1/1	1/1	1/2	1/3	1/5
k1	0.06243	1.06012	0.05966	0.11908	0.10873	0.11010
k2	0.32465	0.07867	0.29474	0.26253	0.26372	0.25186
	$10^4 \leq Gr_1$ and $Gr_1 \leq 10^5$	$10^5 < Gr_1$ and $Gr_1 \leq 7 \times 10^5$	$7 \times 10^5 < Gr_1$ and $Gr_1 \leq 10^8$	$10^4 \leq Gr_1$ and $Gr_1 \leq 10^8$	$10^4 \leq Gr_1$ and $Gr_1 \leq 10^8$	$10^4 \leq Gr_1$ and $Gr_1 \leq 10^8$

Table I.
Values of coefficients k1 and k2 for equation (11) (case 1)

Run	F_r	Gr_2	$\overline{Nu}$	N × M
01	1/1	10^2	1.00	21 × 21
02	1/1	10^4	1.27	31 × 51
03	1/1	10^5	3.24	31 × 51
04	1/1	10^6	5.49	61 × 51
05	1/2	10^2	1.00	21 × 21
06	1/2	10^4	1.66	31 × 51
07	1/2	10^5	3.61	31 × 51
08	1/2	10^6	7.51	31 × 51
09	1/2	10^7	18.44	31 × 51
10	1/3	10^2	1.00	21 × 21
11	1/3	10^4	1.41	31 × 51
12	1/3	10^5	3.21	31 × 51
13	1/3	10^6	6.57	31 × 51
14	1/3	10^7	15.52	31 × 51
15	1/5	10^2	1.00	21 × 21
16	1/5	10^4	1.24	31 × 51
17	1/5	10^5	2.72	31 × 51
18	1/5	10^6	5.34	31 × 51
19	1/5	10^7	11.77	31 × 51

Table II.
Summary of principal runs for case 2

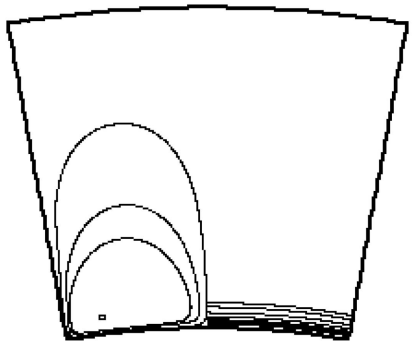

(a) $\tilde{t} = 0.01$

$\tilde{\Omega}$: 0.47, 0.10, 0.05, 0.01

$\tilde{T}$ bottom-->top : 30, 25, 20, 15, 10, 5, 2, 1

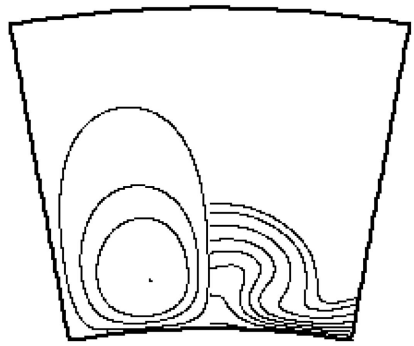

(b) $\tilde{t} = 10$

$\tilde{\Omega}$: 24, 10, 5, 1

$\tilde{T}$ bottom-->top : 30, 25, 20, 15, 10, 5, 2, 1

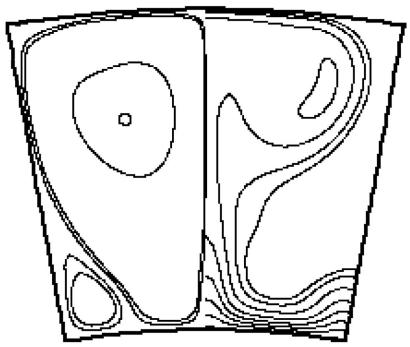

(c) $\tilde{t} = 20$

$\tilde{\Omega}$ (upper cells) : 80, 50, 2, 1

$\tilde{\Omega}$ (lower cells) : -2, -1

$\tilde{T}$ bottom-->top : 30, 25, 20, 15, 10, 5, 2, 1

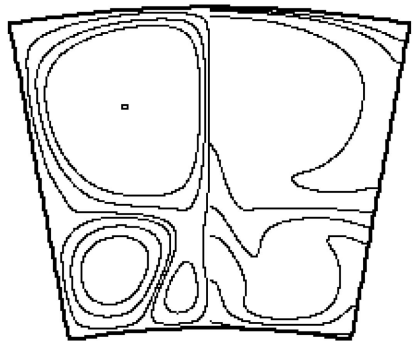

(d) $\tilde{t} = 150$

$\tilde{\Omega}$ (upper cells) : 138.95, 10, 5, 1

$\tilde{\Omega}$ (lower cells, left) : -10, -5, -1

$\tilde{\Omega}$ (lower cells, right) : 5, 1

$\tilde{T}$ bottom-->top : 30, 25, 20, 15, 10, 5, 2, 1

Figure 9.
Variation of streamlines and isotherms versus dimensionless time for $F_r = 1/1$ and for $Gr_1 = 10^6$ (case 2)

The values of the constants k3 and k4, corresponding to the investigated aspect ratios, are presented in Table III according to the application domains of the preceding formula.

Conclusions

We established a mathematical model interpreting the motion transfers inside the fluid and the heat transfers through the active walls of the enclosure. This model rests on the Boussinesq hypothesis and the laminar two-dimensional rate of the flow. The numerical calculation program perfected is based on a finite difference method and allows us to determine the different characteristics of the fluid and the transfer coefficients on the active walls of the enclosure.

This study allowed us to show that, for the two cases of boundary conditions investigated, the nature of the flow is qualitatively the same. This study equally allowed one to display and to quantify the appearance, for high Grashof numbers and for $F_r = 1/1$, of a localized perturbation on the lower

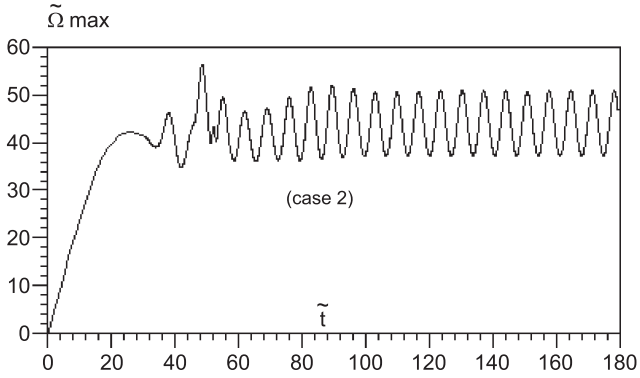

Figure 10.
Variation of maximum stream function versus dimensionless time for $F_r = 1/1$ and for $Gr_2 = 10^6$

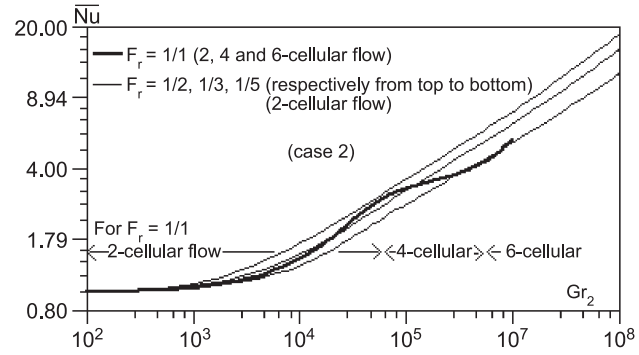

Figure 11.
Mean Nusselt number on isothermal walls versus Grashof numbers for different aspect ratios (log-log scale)

F_r	1/1	1/1	1/1	1/2	1/3	1/5
k3	0.02732	0.66625	0.01198	0.07312	0.05752	0.06131
k4	0.42837	0.13732	0.44353	0.34161	0.34729	0.32618
	$10^4 \leq Gr_2$ and $Gr_2 \leq 6 \times 10^4$	$6 \times 10^4 \leq Gr_2$ and $Gr_2 \leq 5 \times 10^5$	$5 \times 10^5 \leq Gr_2$ and $Gr_2 \leq 10^6$	$10^4 \leq Gr_2$ and $Gr_2 \leq 10^7$	$10^4 \leq Gr_2$ and $Gr_2 \leq 10^7$	$10^4 \leq Gr_2$ and $Gr_2 \leq 10^7$

Table III.
Values of coefficients k3 and k4 for equation (12) (case 2)

corners of the enclosure. This perturbation shows itself by the existence of a thermal relay between the two active walls of the enclosure inside the fluid. With increasing Grashof number, the stable flow changes into the periodic one and then the turbulent flow appears, which can be treated statistically.

References

Al-Ani, N. and Nansteel, M.W. (1993), "Natural convection in partial sector-shaped enclosure: experimental results", *Journal of Heat Transfer*, Vol. 115, pp. 133-9.

Bejan, A. (1984), *Convection Heat Transfer*, A Wiley-Interscience Publication, John Wiley & Sons, New York, NY.

Carnahan, B., Luther, H.A. and Wilkes, J.O. (1969), *Applied Numerical Methods*, Wiley, New York, NY.

Castrejon, A. and Spalding, D.B. (1988), "An experimental and theoretical study of transient free-convection flow between horizontal concentric cylinders", *Int. J. Heat Mass Transfer*, Vol. 31, pp. 27-84.

Fukuda, K., Miki, Y. and Hasegawa, S. (1990), "Analytical and experimental study on turbulent natural convection in a horizontal annulus", *Int. J. Heat Mass Transfer*, Vol. 28 No. 4, pp. 629-39.

Gourdin, A. and Boumahrat, M. (1983), *Méthodes Numériques Appliquées*, Lavoisier TEC & DOC, Paris.

Kumar, K. (1988), "Study of natural convection in horizontal annuli", *Int. J. Heat Mass Transfer*, Vol. 31, pp. 1137-48.

Lavrentiev, M. and Chabat, B. (1972), *Méthodes de la théorie des fonctions d'une variable complexe*, Editions MIR, Moscow.

Peaceman, D.W. and Rachford, H.H. (1955), "The numerical solution of parabolic and elliptic differential equations", *J. Soc. Ind. Appl. Math.*, Vol. 3 No. 1, pp. 28-41.

Rao, Y.F., Miki, Y., Fukuda, K., Tanaka, Y. and Hasegawa, S. (1985), "Flow patterns of natural convection in horizontal cylindrical annuli", *Int. J. Heat Mass Transfer*, Vol. 28, pp. 705-14.

Roache, P.J. (1982), *Computational Fluid Dynamics*, Hermosa Publishers, Albuquerque, NM.

Sarr, J. (1994), "Contribution à l'étude théorique et expérimentale de la convection naturelle transitoire et permanente dans un secteur annulaire", Thèse de Doctorat des Sciences Physiques, Université Cheikh Anta Diop de Dakar.

Sarr, J., Mbow, C., Chehouani, H., Zeghmati, B., Benet, S. and Daguenet, M. (1995), "Study of natural convection in an enclosure bounded by two cylinders and two diametric planes", *Journal of Heat Transfer*, Vol. 117, pp. 130-37.

Vafai, K. and Ettefagh, J. (1991), "An investigation of transient three-dimensional buoyancy-driven flow and heat transfer in a closed horizontal annulus", *Int. J. Heat Mass Transfer*, Vol. 34, pp. 2555-70.